

Elemental Effects on Weld Cracking Susceptibility in $\text{Al}_x\text{CoCrCu}_y\text{FeNi}$ High-Entropy Alloy



ALEXANDER C. MARTIN, JOÃO PEDRO OLIVEIRA, and CAROLIN FINK

Weld solidification and weldability of $\text{Al}_x\text{CoCrCu}_y\text{FeNi}$ high-entropy alloys (HEA) were characterized as a function of Al and Cu molar ratio in the alloy composition. Autogenous gas tungsten arc welding (GTAW) was performed on the as-melted ingots. Fusion zone and heat-affected zone microstructures were investigated using optical and electron microscopy, and compared to thermodynamic CALPHAD-based calculations. Weld cracking susceptibility was compared to cast pin tear test (CPTT) results. It was found that strong Cu segregation on solidification promotes hot cracking in fusion welds on $\text{AlCoCrCu}_y\text{FeNi}$ alloys ($y > 0.1$). Cu-rich liquid forms during the final stages of solidification and facilitates solidification cracking in the fusion zone. The Cu-rich interdendritic readily remelts during reheating and promotes liquation cracking in the heat-affected zone. The cracking mechanisms in the welds change to brittle intergranular cracking in low and no Cu alloy compositions due to a high-hardness BCC microstructure (> 500 HV). Lowering the Al molar ratio in $\text{Al}_x\text{CoCrCu}_{0.1}\text{FeNi}$ alloys ($x \leq 0.5$) mitigates brittle cracking by promoting FCC solidification structure.

<https://doi.org/10.1007/s11661-019-05564-8>

© The Minerals, Metals & Materials Society and ASM International 2019

I. INTRODUCTION

THE concept of high-entropy alloys (HEA) introduced a new way of advanced materials development. High-entropy alloys are defined as multi principal element alloys usually composed of five or more alloying elements (from 5 to 35 at. pct each).^[1] This is radically different from conventional micro-alloying strategies enabling properties that far-surpass that of conventional alloys. Until recently, most HEA research aimed to provide a fundamental understanding of high-entropy alloy processing, microstructures, and mechanical behavior. The focus is shifting to more carefully designed high-entropy alloys that possess multiple phases and tailored microstructures in order to achieve a unique set of properties relevant to specific industrial applications.^[2] However, an engineering design approach imposes additional constraints onto the HEA development process. Besides good mechanical behavior, structural applications may require many other properties, including the ability to be joined and formed into complex shapes.^[3] Welding is a critical

manufacturing process for structural components. Therefore, it is essential to address the weldability of candidate structural high-entropy alloys in the alloy development process. This can enable enhancement of weld properties, and early avoidance of adverse issues related to welding by modification of composition or microstructures during an application-driven HEA design. Little attention has been paid to high-entropy alloy welding metallurgy and weldability. Non-equilibrium conditions will significantly alter microstructures and weld properties in the fusion zone and heat-affected zone in these materials, but have not yet studied in detail.

High-temperature applications are particularly interesting for alloy development based on the high-entropy concept. Among several types, the AlCoCrCuFeNi alloy system has been studied in detail due to some alloy compositions exhibiting thermal stability of microstructure and strength retention up to temperatures of 800 °C.^[1,4,5] High elevated temperature strength and good wear resistance make these alloys potential candidates for applications in structural and tool industries.^[5] $\text{Al}_x\text{CoCrCu}_y\text{FeNi}$ alloys (x and y values in molar ratio) show a gradual change from single FCC phase to mixed FCC and BCC phase, and to single BCC phase with increasing Al content. This structural change is accompanied by a significant increase in hardness.^[5,6] Copper was found to strongly segregate in this alloy system due to its high enthalpy of mixing with other elements.^[7,8] This shifted emphasis to alloy compositions with low Cu content or without Cu.^[4,9,10] Few studies have looked at

ALEXANDER C. MARTIN and CAROLIN FINK are with the Department of Material Science and Engineering, Welding Engineering Program, The Ohio State University, 1248 Arthur E. Adams Drive, Columbus, OH 43221. Contact e-mail: fink.242@osu.edu JOÃO PEDRO OLIVEIRA is with the Department of Mechanical and Industrial Engineering, New University of Lisbon, 2829-516 Caparica, Portugal.

Manuscript submitted June 26, 2019.

Article published online December 4, 2019

the microstructural evolution in $\text{Al}_x\text{CoCrCu}_y\text{FeNi}$ alloys during welding or welding-related processing. Solidification was dendritic when cooled fairly slowly using arc or levitation melting.^[7,11] Higher cooling rate processes, *i.e.*, laser and electron beam (EB) surface remelting^[12,13] and direct laser deposition of alloy powders,^[14,15] resulted in fine dendritic fusion zone structures and less amount of Cu-rich interdendritic regions in Cu-containing alloy compositions. Increased hardness in the fusion zone was observed after EB remelting of $\text{Al}_x\text{CoCrFeNi}$ alloys.^[12] The same study reported a high tendency for fusion zone and heat-affected zone cracking in deep penetration welds and multi-pass surface remelts on the high Al composition ($x = 0.8$), while no cracking was observed in the lower Al composition ($x = 0.6$). It was hypothesized that the cracking is associated with the higher hardness at increased Al content, but no further characterization on the type of cracking was performed.^[12]

The present study aims for a more comprehensive characterization of the welding metallurgy and weldability of the $\text{Al}_x\text{CoCrCu}_y\text{FeNi}$ alloy system. In this initial approach, autogenous gas tungsten arc welding (GTAW) was performed on the as-melted microstructures, which essentially depicts a worst-case scenario seen in repair and multi-pass weld situations, as well as advanced fusion-based additive processing. Fusion zone and heat-affected zone microstructures were characterized using optical and electron microscopy. Thermodynamic CALPHAD-based (CALculation of PHase Diagrams) calculations were performed to investigate constituent phases on non-equilibrium solidification, and critically assess the predictive capabilities of the CALPHAD approach for this high-entropy alloy system. The cast pin tear test (CPTT) was used to evaluate resistance to weld cracking as a function of alloy composition. This paper seeks to provide a reference study for further investigations on an alloy composition optimized for weld applications.^[16]

II. EXPERIMENTAL

HEA ingots (10 g) of $\text{Al}_x\text{CoCrCu}_y\text{FeNi}$ (*i.e.*, $x = 0.5$ and 1.0, and $0 \leq y \leq 1.0$ in molar ratio) nominal composition were prepared by arc melting of high-purity (≥ 99.9 pct) constituent elements. Melting was done under argon atmosphere after purging five times to prevent oxidation. Ingots were remelted three times to improve chemical homogeneity.

Solidified ingots were subjected to autogenous gas tungsten arc (GTA) welding using a stationary welding torch at an arc voltage of 11 V and a welding current of 120 A. Welding parameters were selected to result in cooling rates in the solidifying weld pool that resemble those commonly seen in gas tungsten arc welding (about 200 K/s).^[17]

Alloy compositions were evaluated for resistance to weld solidification cracking using the cast pin tear test (CPTT). Details of the test procedure can be found in Reference 18. Three pins were cast for each alloy

composition at 12.7 mm (0.5 in.) mold length. Test parameters used have been described in Reference 16.

The as-melted ingots and gas tungsten arc welds were sectioned and prepared for optical and electron microscopy using standard metallographic procedures. Polished surfaces were submerged in molybdenum solution (100 mL H_2O , 100 mL HNO_3 , and 3 g H_2MoO_4) for 3-5 seconds.^[19] Secondary electron microscope (SEM) imaging and compositional analysis *via* X-ray energy dispersive spectroscopy were performed in a Quanta 200 system. MIPAR software package^[20] was used to determine fraction of interdendritic phase in the solidified microstructure on a minimum of three light optical micrographs (1000 \times). Vickers hardness was measured with 200 and 500 g loads and 12-second dwell time.

Thermo-Calc software version 2018a with TCHEA3 High-Entropy Alloy database was used for CALPHAD-based solidification calculations. TCHEA3 database describes a 26-element framework and includes thermodynamic data for almost all binary subsystems and hundreds of ternaries (> 400). Calculations were performed in order to predict phase formation and partitioning under equilibrium and non-equilibrium (Scheil) solidification, associated solidification path, solidification temperature range, and constituent phases at the end of solidification. The solidification temperature range (STR) is often used to evaluate the susceptibility to weld solidification cracking. It was taken as the difference between the solidification start temperature, and the solidification finish temperature at a fraction solid (f_s) of 0.95. The partition coefficient (k) describes how strongly alloying elements partition to the liquid and solid phases during solidification. It is formally defined as the composition of the solid (C_s) divided by the composition of the liquid (C_l) at a particular temperature. For k values < 1 , the final degree of micro-segregation in the as-solidified microstructure increases with decreasing k value. Partition coefficients close to unity ($k \approx 1$) indicate almost no tendency for partitioning during solidification. Details on parameters used for Scheil calculations can be found in Reference 16. Solidification calculations were performed for all experimentally prepared alloy compositions.

III. RESULTS AND DISCUSSION

A. As-Melted Microstructures of $\text{Al}_x\text{CuCrCu}_y\text{FeNi}$ Alloy System

Figure 1(a) reveals the as-melted microstructure of equiatomic alloy composition AlCoCrCuFeNi . The light optical micrograph shows the dendritic structure in the as-polished condition (no etching). Evidence of solute segregation is clearly distinguishable within the solidification structure. Chemical analysis (XEDS), shown in Figures 1(c) and (d), reveals interdendritic regions highly enriched in Cu. All other constituent elements are depleted as compared to the dendrite composition. However, there is a noticeable enrichment

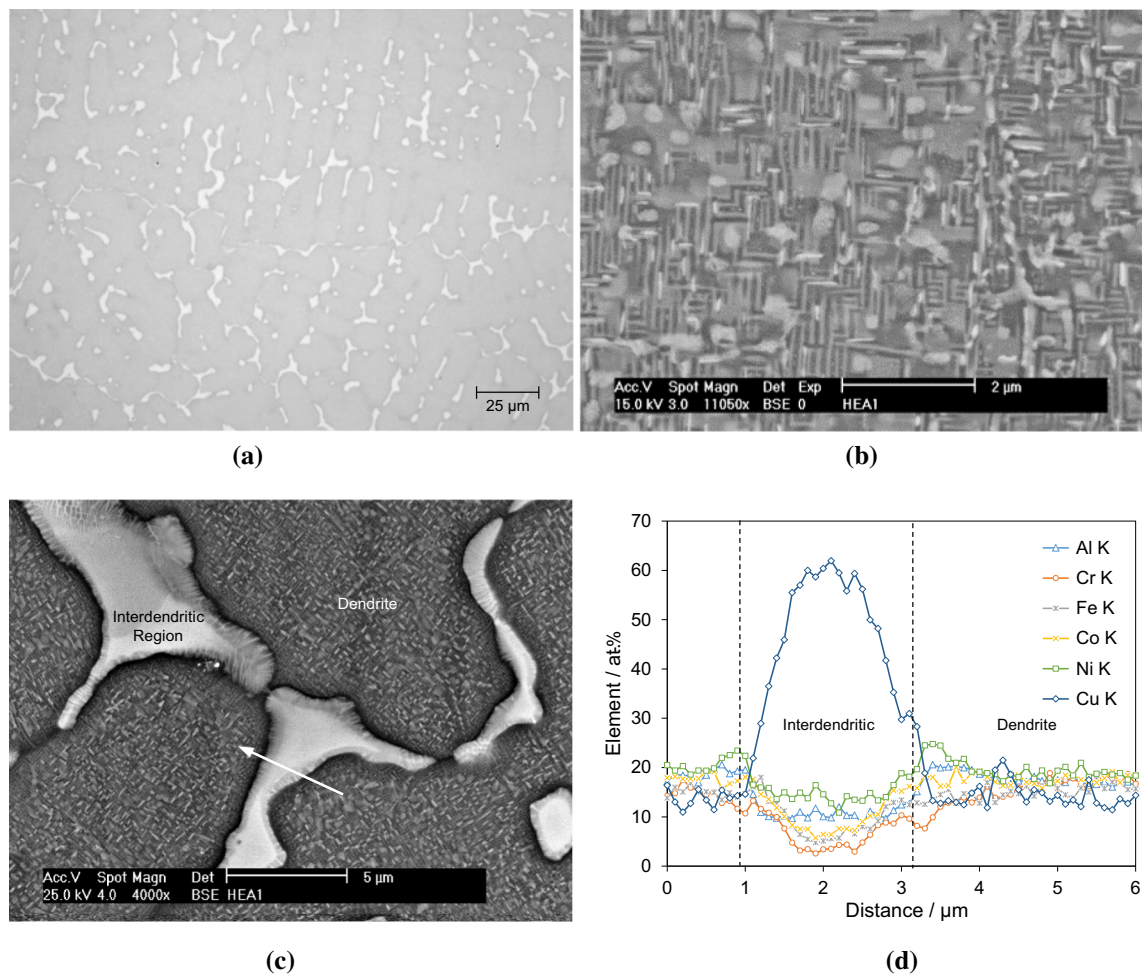


Fig. 1—As-melted microstructure of equiatomic AlCoCrCuFeNi: (a) Light optical micrograph in the as-polished condition, (b) SEM (BSE) image of dendrite region, (c) and (d) SEM image and compositional profile (XEDS) across interdendritic region (arrow).

of Al and Ni towards the edges of the dendritic phase, see Figure 1(d). Strong partitioning of Cu has been reported in this alloy system due to the high positive mixing enthalpy of Cu with Fe, Cr, Co, and Ni.^[7] In addition, Wang *et al.*^[6] suggested that Al and Ni atoms are repelled continuously from the dendrite matrix during solidification, and accumulate as an Al-Ni-rich layer between the dendrite and interdendritic regions.

Figure 1(b) presents a representative backscatter electron micrograph of the dendrite microstructure. The dendritic regions solidify as body-centered cubic (BCC) phase.^[7] The complex modulated microstructure seen in Figure 2(b) has been attributed to the occurrence of spinodal decomposition into ordered Al-Ni-rich plates (B2) and disordered Cr-Fe-rich BCC (A2) interplates.^[6,7,11] The bright elongated constituents in Figure 1(b) are several types of nano-sized Cu-rich precipitates that have been previously reported for this alloy composition^[11] and were not further analyzed in this study. The interdendritic regions, shown in Figure 1(c), were reported to be primarily composed of face-centered cubic (FCC) Cu-rich phase, and some

BCC plate-interplate structure formed by spinodal decomposition.^[11]

Figure 2 shows the as-melted microstructures (light optical micrographs) of $\text{Al}_x\text{CoCrCu}_y\text{FeNi}$ alloys with Al ($x = 0.5$ and 1.0) and Cu ($0 \leq y \leq 1.0$) in different molar ratios. Equiatomic alloy AlCoCrCuFeNi, shown in Figure 2(a), forms a cellular BCC dendritic structure with a high-volume fraction of Cu-rich FCC phase in the interdendritic regions. Decreasing Cu molar ratio in this alloy system reduces the amount of Cu-rich interdendritic phase, as shown in Figures 2(a) through (d). This is consistent with disappearing FCC reflection peaks in X-ray diffraction on low Cu compositions ($y \leq 0.5$).^[8] It can also be seen in Figure 2 that the solidification structure coarsens with decreasing molar ratio of Cu in the alloy composition. The solidification mode shifts from a cellular dendritic to an equiaxed dendritic grain structure for AlCoCrCu_{0.1}FeNi and AlCoCrFeNi alloys, shown in Figures 2(d) and (e), respectively.

Lowering the molar ratio of Al ($x = 0.5$) in the alloy system results in a fine cellular dendritic microstructure

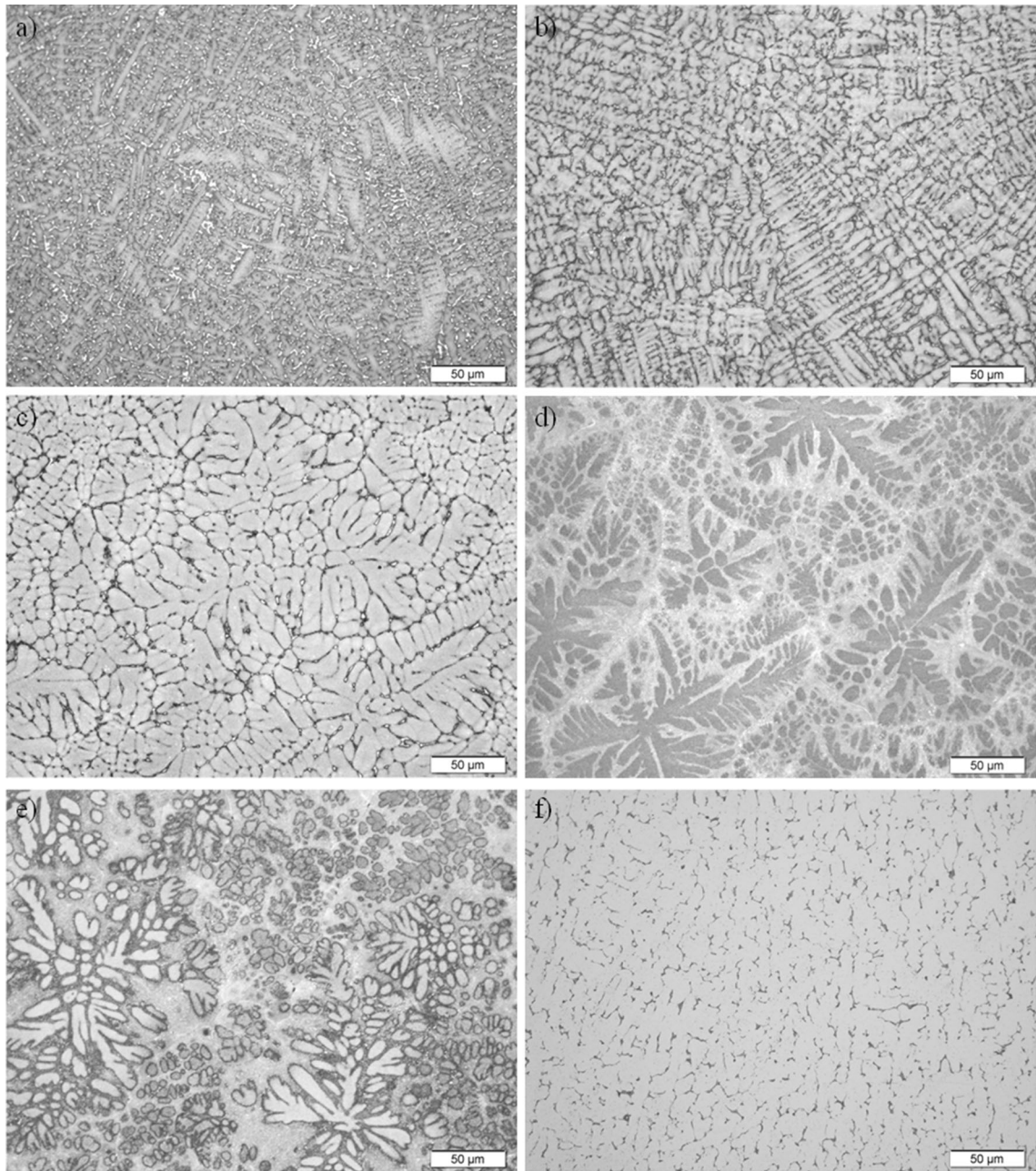


Fig. 2—As-melted microstructures as a function of Cu and Al additions: (a) AlCoCrCuFeNi, (b) AlCoCrCu_{0.5}FeNi, (c) AlCoCrCu_{0.3}FeNi, (d) AlCoCrCu_{0.1}FeNi, (e) AlCoCrFeNi, and (f) Al_{0.5}CoCrCu_{0.1}FeNi. Light optical micrographs etched with molybdenum solution.

with distinct interdendritic regions, compare Al_xCoCrCu_{0.1}FeNi alloys in Figures 2(d) and (f). Al_{0.5}CoCrCu_{0.1}FeNi has a hardness of 208 HV0.2, which is significantly lower than that of the other alloys in this study (> 500 HV0.5, see Table I). This is due to the fact that the dendrite core regions in the low Al compositions ($x \leq 0.5$) have an FCC structure, whereas BCC dendrites with an ordered structure form in all other alloy compositions. It has been previously reported that Al facilitates the formation of BCC phase in this alloy system and enhances the ordering of the BCC structure.^[6–8] Table I summarizes the observed solidification

morphology, and shows the measured Vickers hardness for all alloy compositions.

B. Scheil Solidification Calculations

Figure 3 (left) presents solidification calculations from equilibrium and Scheil simulation for equiatomic alloy composition AlCoCrCuFeNi. The calculation predicts solidification to start from two liquid phases, one of which is a Cu-rich liquid phase that persists until the end of solidification at about 950 °C. The Scheil solidification path suggests primary BCC solidification

Table I. Solidification Morphology and Vickers Hardness of Al_xCoCrCu_yFeNi Alloys

Alloys	Solidification Morphology	Hardness (HV)
AlCoCrCuFeNi	cellular dendritic	526 ± 8
AlCoCrCu _{0.5} FeNi	cellular dendritic	574 ± 8
AlCoCrCu _{0.3} FeNi	cellular dendritic	577 ± 8
AlCoCrCu _{0.1} FeNi	equiaxed dendritic	504 ± 5
AlCoCrFeNi	equiaxed dendritic	527 ± 7
Al _{0.5} CoCrCu _{0.1} FeNi	cellular dendritic	208 ± 5

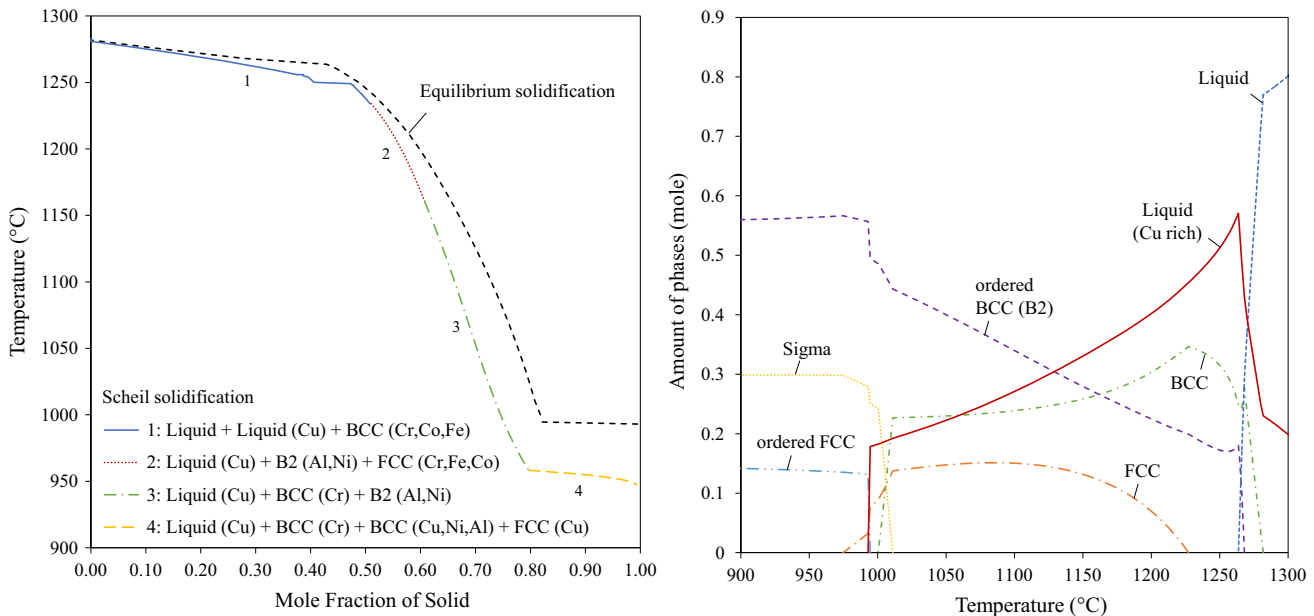


Fig. 3—Equilibrium and Scheil solidification calculations (left), and equilibrium property diagram from step-calculation (right) for equiatomic AlCoCrCuFeNi.

(Cr-Co-Fe-rich phase), and subsequent solidification of Al-Ni-rich BCC (B2) and Cr-Co-Fe-rich FCC phases. Solidification is predicted to terminate with the formation of primarily Cu-rich FCC phase in the interdendritic regions. The step-calculation in Figure 3 (right) shows the phase formation under equilibrium condition as mole fraction of stable phases as a function of temperature. It can be seen that the separation of a Cu-rich liquid is predicted to persist down to about 1000 °C. No single-phase region exists below the melting range. The alloy is predicted to consist of ordered Al-Ni-rich BCC (B2) phase, ordered Cu-rich FCC phase, and Sigma phase. The thermodynamic calculations are in good agreement with the experimentally observed solidification microstructure of equiatomic AlCoCrCuFeNi alloy in this study (Figure 1), and literature findings on phase formation in aged microstructures of AlCoCrFeNi alloy.^[4]

Calculated partition coefficients (k) from Scheil solidification data are shown in Figure 4. Co, Cr, and Fe have partition coefficients $k \gg 1$, which indicates partitioning to the dendrite core during solidification. Cu ($k \ll 1$) is expected to segregate very strongly to the cell/dendrite boundaries, while Al and Ni ($k < 1$) exhibit

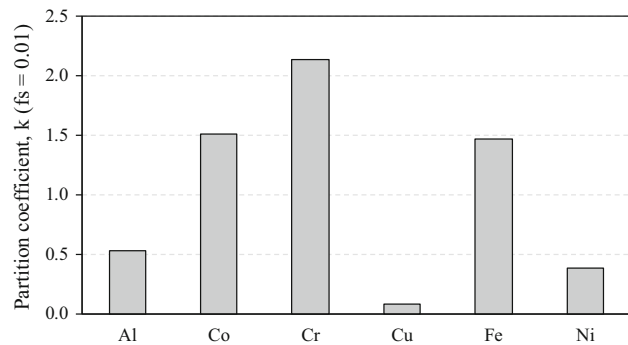


Fig. 4—Calculated partition coefficients (k) at fraction solid of 0.01 (beginning of solidification). For k values > 1 , segregation occurs towards the dendrite core, and for k values < 1 , the element will segregate towards the cell/dendrite boundary.

a moderate tendency for segregation. The values shown in Figure 4 represent k at the start of solidification ($f_s = 0.01$). The data do not take into account variations in k during solidification as function of decreasing temperature. However, the partition coefficient of Cu (k_{Cu}) never exceeds values of $k = 0.2$, when plotted across the whole solidification temperature range. This

indicates a strongly segregated microstructure, and is consistent with the steep Cu gradient across the dendritic substructure shown in Figure 1(d). The experimentally observed segregation of Al and Ni is also in good agreement with their predicted moderate tendency for segregation during solidification.

The Cu-rich liquid that is predicted both under equilibrium and Scheil conditions (Figure 3) results in a wide solidification temperature range (300 K-350 K) for equiatomic alloy composition AlCoCrCuFeNi. Lowering the Cu molar ratio in the AlCoCrCu_yFeNi alloy system changes the shape of the predicted Scheil solidification curve, as shown in Figure 5. The curve is steeper in the final stages of solidification with decreasing Cu molar ratio, which indicates a smaller amount of liquid phase present at the end of solidification, and a narrower solidification temperature range for low Cu compositions. Table II compares the solidification start and finish temperatures, and the solidification temperature range for alloy compositions with varying Cu molar ratio ($y = 1.0, 0.5, 0.3$ and 0.1). AlCoCrCu_{0.1}FeNi is characterized by the smallest solidification temperature range (162 K) at 0.95 fraction solid (f_s).

Figure 6 shows the effect of Al molar ratio ($x = 1.0, 0.8, 0.5$ and 0.3) on the phase fractions present at the end of solidification in Al_xCoCrCu_{0.1}FeNi alloys. It can

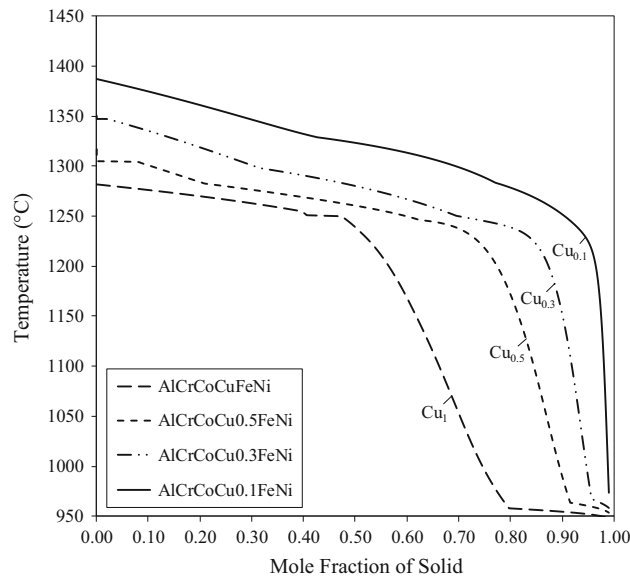


Fig. 5—Scheil solidification calculations for AlCoCrCu_yFeNi alloys with different Cu molar ratios ($y = 1.0, 0.5, 0.3$ and 0.1).

Table II. Solidification Start and Finish Data from Scheil Calculations

Alloys	Solidification Start Temperature (°C)	Solidification Finish Temperature ($f_s = 0.99$) (°C)	Solidification Finish Temperature ($f_s = 0.95$) (°C)	Solidification Temperature Range (STR) ($f_s = 0.95$) (°C)
AlCoCrCuFeNi	1282	947	952	330
AlCoCrCu _{0.5} FeNi	1304	953	960	345
AlCoCrCu _{0.3} FeNi	1347	958	989	358
AlCoCrCu _{0.1} FeNi	1387	974	1224	162

be seen that Al is predicted to promote the formation of BCC phase in the solidified microstructure. Low Al composition Al_{0.3}CoCrCu_{0.1}FeNi exhibits an almost completely FCC structure on Scheil solidification. The predicted change from FCC to BCC crystal structure with increasing Al content is consistent with experimental results in the literature.^[6-8]

C. Autogenous Gas Tungsten Arc Welding

Figure 7(a) shows the fusion line and heat-affected zone region of an autogenous gas tungsten arc (GTA) weld on an arc-melted ingot of equiatomic alloy composition AlCoCrCuFeNi. Weld solidification occurs by epitaxial nucleation and growth at the fusion line. The fusion zone exhibits a much finer dendritic structure as compared to the arc-melted ingot microstructure, caused by the higher cooling rate of the stationary GTA weld. Cu strongly segregates to the interdendritic regions during weld solidification due to its very low k value (see Figure 4). Small liquation cracks ($\leq 500 \mu\text{m}$) were observed in the heat-affected zone (HAZ) adjacent to the fusion line. The cracks propagate along the interdendritic regions of the reheated ingot microstructure, as shown in Figure 7(b). The Cu-rich interdendritic readily melts upon reheating in the high-temperature HAZ, since its melting occurs at temperatures below 1000°C (see Figure 3). Liquation cracking occurs within this partially melted zone (PMZ) when the Cu-rich liquid locally cannot sustain the mechanically and/or thermally induced restraint imposed during the welding process. No cracking was observed in the weld fusion zone, probably due to its finer solidification microstructure and lower amount of Cu-rich interdendritic.

Figure 8 presents cross sections of autogenous GTA welds on arc-melted ingots of AlCoCrCu_yFeNi alloys with varying Cu molar ratios ($y = 0.5, 0.3, 0.1$, and 0). All alloy compositions exhibit some degree of macroscopic cracking (up to 2.5 mm crack length) throughout the fusion zone and HAZ. Figure 9(a) illustrates the interdendritic crack path observed in AlCoCrCu_{0.5}FeNi and AlCoCrCu_{0.3}FeNi, in which cracking is most severe, as seen in Figures 8(a) and (b), respectively. Cu-rich phase is readily apparent along the interdendritic separations in the fusion zone and HAZ microstructures. Most of the cracks run across the fusion line, which indicates a liquation cracking mechanisms with crack initiation in the HAZ. Unlike in equiatomic AlCoCrCuFeNi, cracking in AlCoCrCu_{0.5}FeNi and

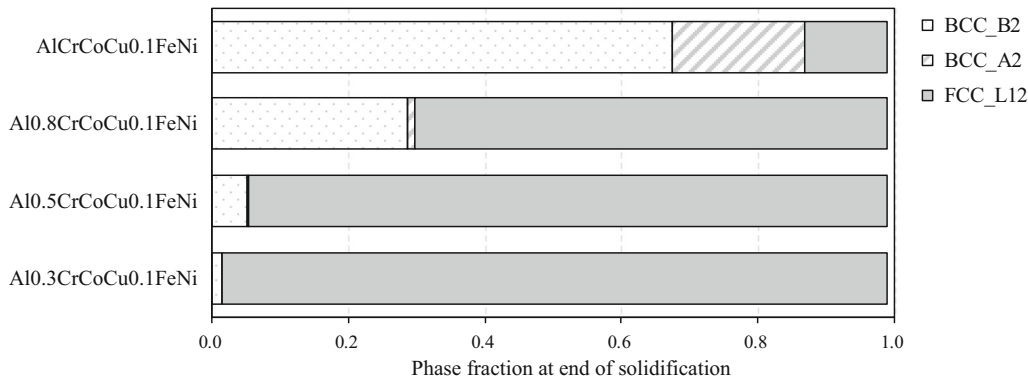


Fig. 6—Calculated phase fractions at the end of (Scheil) solidification for $\text{Al}_x\text{CoCrCu}_{0.1}\text{FeNi}$ alloys with different Al molar ratios ($x = 1.0, 0.8, 0.5,$ and 0.3).

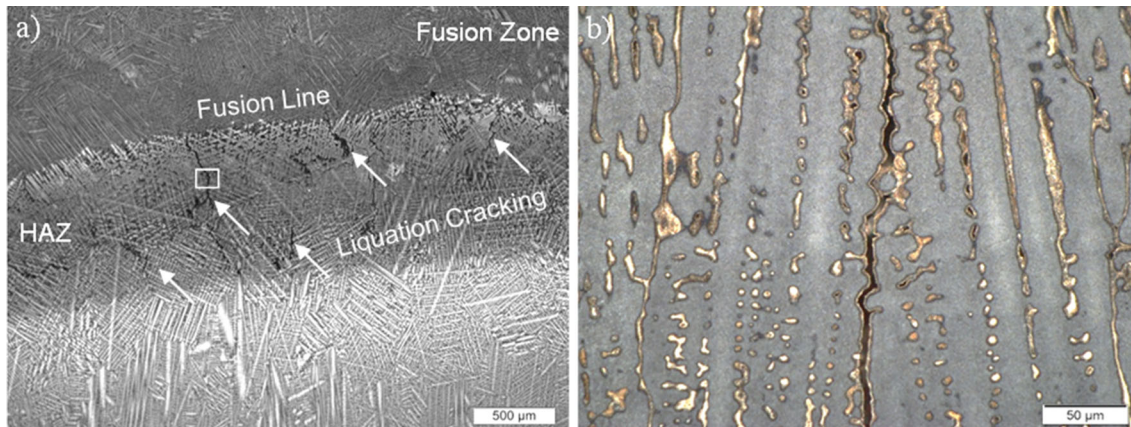


Fig. 7—Light optical micrographs from cross-sectioned autogenous gas tungsten arc (GTA) weld on equiatomic AlCoCrCuFeNi : (a) Overview of the fusion line and heat-affected zone (HAZ) region, and (b) detail of HAZ cracking along Cu-rich interdendritic region (yellow color) (Color figure online).

$\text{AlCoCrCu}_{0.3}\text{FeNi}$ is not contained within the HAZ, but extends far into the fusion zone, probably due to its coarser dendritic structure. Less severe cracking was observed in the GTA welds on $\text{AlCoCrCu}_{0.1}\text{FeNi}$ and AlCoCrFeNi , as seen in Figures 8(c) and (d), respectively. Higher magnification micrographs revealed that the cracking in these welds is transgranular. Figure 9(b) shows a typical crack path cutting through the dendritic structure in the HAZ of AlCoCrFeNi . Most of the observed cracking runs across the fusion line, and extends far into the fusion zone and HAZ. SEM imaging of the fracture surface topography confirmed the transgranular nature of the cracking in both the fusion zone and HAZ (Figure 10). The fracture surface features steps and river patterns on individual facets, topographic features that are characteristic for quasi-cleavage fracture mode. Quasi-cleavage fracture is often associated with hard brittle microstructures. In fact, the microhardness of $\text{AlCoCrCu}_{0.1}\text{FeNi}$ and AlCoCrFeNi exceeds 500 HV0.5 (see Table I). Interestingly, Figure 10 shows a small region of intergranular fracture along the fusion line. This might indicate that crack initiation happened along grain boundaries close to the fusion line in the high-temperature HAZ, and cracks propagated transgranular through the fusion zone and

HAZ. Smooth grain surfaces and a lack of microductility point to liquid film formation in the partially melted zone (PMZ) as a possible mechanism for the observed intergranular fracture close to the fusion line. Liquation originates from local remelting of the interdendritic regions in the arc-melted ingot microstructure. The degree of liquation is quite small, since there is little evidence of the resolidified liquid on the individual grain surfaces. No Cu-rich interdendritic phase is predicted to form in $\text{AlCoCrCu}_{0.1}\text{FeNi}$ and AlCoCrFeNi during Scheil solidification. However, the partitioning of Al and Ni into the liquid during solidification ($k < 1$) might lower the effective melting temperature locally in the interdendritic regions, and enable liquid film formation upon reheating.

D. Cast Pin Tear Testing

Results of the cast pin tear test (CPTT) are presented in Figure 11 as average circumferential cracking observed over all tested pins. Testing was performed at a single mold length of 12.7 mm (0.5 in.). Restraint during solidification and hence severity of testing conditions increases with increasing mold length. For reference, conventional Ni-base alloys, which are

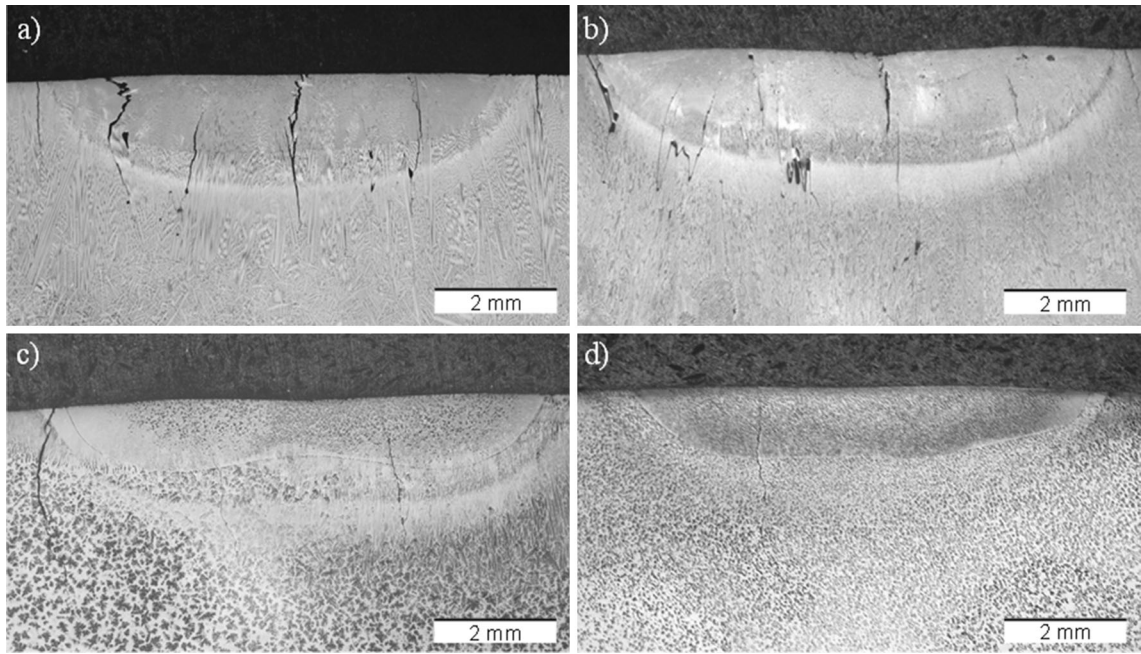


Fig. 8—Cross sections (LOM) of autogenous gas tungsten arc (GTA) welds with cracking in the fusion zone and heat-affected zone (HAZ) of (a) AlCoCrCu_{0.5}FeNi, (b) AlCoCrCu_{0.3}FeNi, (c) AlCoCrCu_{0.1}FeNi, and (d) AlCoCrFeNi.

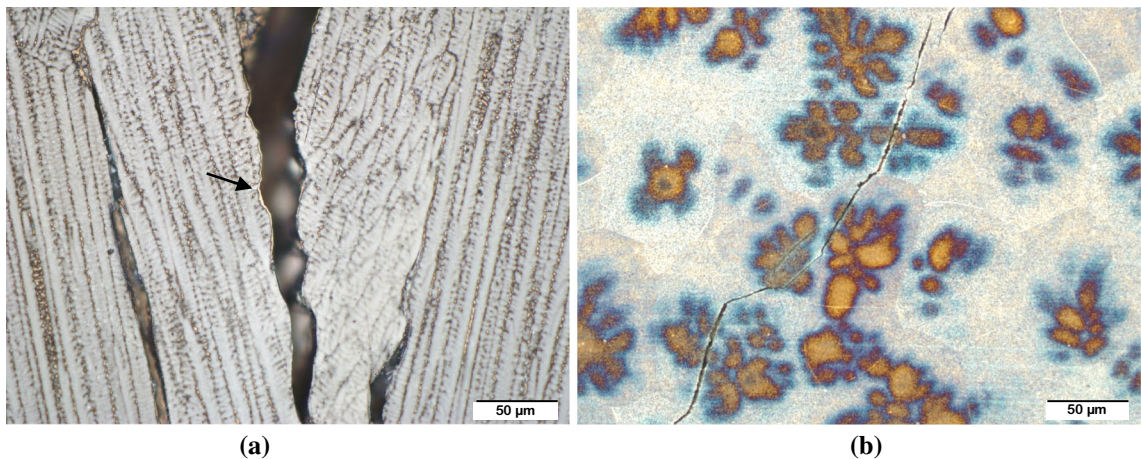


Fig. 9—Higher magnification LOM micrographs of the cracking and associated microstructures in the autogenous gas tungsten arc (GTA) welds: (a) Interdendritic cracking in the fusion zone of AlCoCrCu_{0.5}FeNi, and (b) transgranular cracking in the heat-affected zone (HAZ) of AlCoCrFeNi.

generally considered somewhat susceptible to weld hot cracking, typically exhibit no cracking up to 25.4 mm (1 in.) mold length or higher. As shown in Figure 11, AlCoCrCu_yFeNi alloy compositions with high and medium Cu molar ratios ($y = 1.0, 0.5,$ and 0.3) showed complete (100 pct) circumferential cracking in all tested pins. This severe cracking at 2.7 mm (0.5 in.) mold length indicates a high cracking susceptibility. Based upon the presented characterization of the solidification microstructures and results from solidification modeling, cracking in these compositions is associated with Cu segregation during solidification lowering the effective solidus temperature. Correspondingly, fractography of the cast pins revealed interdendritic fracture with

evidence of liquid film formation. The amount of cracking seen in the cast pins starts to decrease in low Cu composition AlCoCrCu_{0.1}FeNi, and drops further in AlCoCrFeNi (see Figure 11). Metallographic examination showed that cracking in these cast pins runs transgranular through the solidification structure with no liquation involved. This observation matches what was seen in the autogenous gas tungsten arc (GTA) welds on these alloy compositions, where transgranular cracking was attributed to the high-hardness, brittle microstructure. Similar to the small amount of intergranular cracking observed at the fusion line in the GTA welds, it is hypothesized that small solidification cracks initially occur on the surface of the cast pins and act as

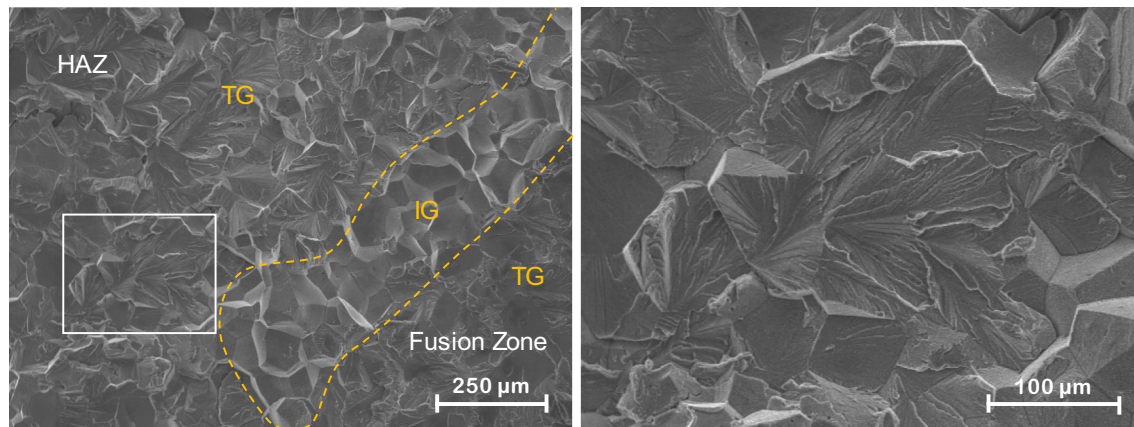


Fig. 10—Fracture surface topography of cracking running across the fusion line in autogenous gas tungsten arc (GTA) weld on AlCoCrFeNi. SEM image. Dashed line indicates region of intergranular (IG) crack propagation across the fusion line as compared to primarily transgranular (TG) cracking in the heat-affected zone and fusion zone. Detail shows steps and river pattern on individual facets indicating quasi-cleavage fracture mode.

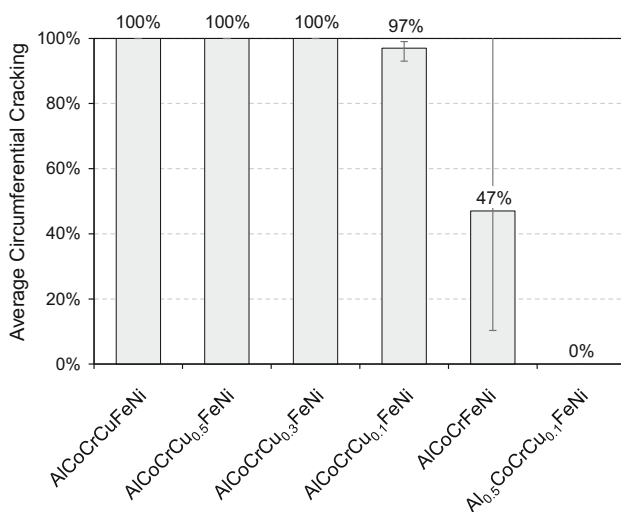


Fig. 11—Cast pin tear test (CPTT) results of Al_xCoCrCu_yFeNi alloys with different Al and Cu molar ratios ($x = 0.5$ and 1.0) and ($0 \leq y \leq 1.0$). Testing performed at 12.7 mm (0.5 in.) mold length.

stress concentrators. Strain build-up during cooling then leads to transgranular fracture through the brittle microstructure of the pins. Figure 11 presents CPTT data for an additional alloy composition, Al_{0.5}CoCrCu_{0.1}FeNi, which was developed by Martin and Fink^[16] in order to improve weldability in this HEA system. This composition exhibited the lowest cracking susceptibility in the CPTT with no cracking at 12.7 mm (0.5 in.) mold length. The reduction in Cu molar ratio ($y = 0.1$) mitigates solidification cracking by limiting the amount of segregation during solidification. Lowering Al ($x = 0.5$) avoids brittle cracking in the cast pins due to a decreased hardness of the primarily FCC microstructure. Detailed characterization of the solidification behavior, thermodynamic modeling, and weldability evaluation of Al_{0.5}CoCrCu_{0.1}FeNi alloy can be found in Reference 16.

IV. CONCLUSIONS

- (1) Weld solidification of equiatomic alloy Al_xCoCrCu_yFeNi ($x = 1.0$, $y = 1.0$) results in a cellular dendritic BCC structure with a high-volume fraction of Cu-rich FCC interdendritic. Decreasing Cu molar ratio in the alloy composition reduces the amount of interdendritic phase, and coarsens the solidification structure. The solidification mode shifts from cellular dendritic to equiaxed dendritic for low and no Cu compositions ($y = 0.1$ and 0).
- (2) Strong segregation of Copper during weld solidification promotes hot cracking in fusion welds on Al_xCoCrCu_yFeNi alloys ($y > 0.1$). Cu-rich liquid forms during the final stages of solidification lowering the effective solidus temperature of the interdendritic regions. The inability of this liquid to accommodate welding-induced restraint results in the formation of solidification cracking in the fusion zone. The Cu-rich interdendritic easily melts upon reheating and enables liquid film formation that promotes liquation cracking in the heat-affected zone during multi-pass or repair welding.
- (3) Aluminum promotes a high-hardness (> 500 HV) BCC solidification microstructure in Al_xCoCrCu_yFeNi alloys ($x > 0.5$), which facilitates brittle fracture (transgranular cracking) during fusion welding. Fractography showed a small region of intergranular fracture mode adjacent to the fusion line, which indicates that cracking might initiate along grain boundaries in the partially melted zone, and propagates transgranular through the hard, brittle microstructure of the fusion zone and heat-affected zone.
- (4) Thermodynamic calculations of phase formation during Scheil solidification used TCHEA3 database in *Thermo-Calc* software, and showed good agreement with experimentally observed solidification microstructures in the Al_xCoCrCu_yFeNi

system. In particular, the calculations predict heavy partitioning of Cu ($k_{\text{Cu}} \ll 1$) into the final liquid during solidification in Cu-containing alloy compositions, and the formation of a hard brittle BCC microstructure at high Al molar ratio ($x > 0.5$).

- (5) Autogenous stationary GTA welding on arc-melted ingots was used as a screening technique for weldability, in particular to assess the cracking susceptibility of AlCoCrCu_yFeNi alloys. The results are in good agreement with cast pin tear test (CPTT) results. The cracking mechanism changes from intergranular liquid film separation (hot cracking) in medium and high Cu compositions ($y > 0.1$) to brittle transgranular fracture mode in low and no Cu alloys. Decreasing Cu and Al molar ratio mitigates both types of cracking in fusion welding of Al_{0.5}CoCrCu_{0.1}FeNi alloy.

The authors would like to point out some limitations of this preliminary study. First, the weldability study performed here attempts to quantify the materials inherent resistance to weld cracking. Joint design, restraint, and welding process and parameters will also play a large role in weld cracking susceptibility. However, starting with an alloy composition that has inherently good cracking resistance in the weld fusion zone and heat-affected zone allows for a higher degree of freedom in weld design and parameter selection. Second, it is important to note that in this study, the composition with the most favorable weldability has a softer FCC matrix as compared to higher strength BCC compositions in this alloy system. However, an increase in hardness in Al_{0.5}CoCrCu_{0.1}FeNi alloy can be achieved upon subsequent precipitation heat treatment due to the formation of strengthening BCC (B2) phase in the dendrite matrix and interdendritic regions.^[16] Lastly, this study lays out a methodology using combined experimental and computational techniques to rapidly evaluate candidate alloy weldability. The high-entropy alloy system studied here has been well characterized in the literature, and microstructures and computational results from this study are in good agreement with previously published results. This high-throughput approach will be used to explore a much wider range of chemistries in this system and others in order to identify alloys with combined properties of good weldability and desired matrix-precipitate phase balance that satisfies strength requirements for structural applications.

ACKNOWLEDGMENTS

This work was supported by the Institute of Materials Research (IMR) at The Ohio State University, and by the American Welding Society (AWS) Foundation. The authors express their gratitude to Brady Soulivong, high school intern in the Welding Engineering Program at The Ohio State University. Electron microscopy was performed at the Center for Electron Microscopy and Analysis (CEMAS) at The Ohio State University.

REFERENCES

1. J.-W. Yeh, S.-K. Chen, S.-J. Lin, J.-Y. Gan, T.-S. Chin, T.-T. Shun, C.-H. Tsau, and S.-Y. Chang: *Adv. Eng. Mater.*, 2004, vol. 6, pp. 299–303.
2. M.-H. Tsai and J.-W. Yeh: *Mater. Res. Lett.*, 2014, vol. 2, pp. 107–23.
3. D.B. Miracle and O.N. Senkov: *Acta Mater.*, 2017, vol. 122, pp. 448–511.
4. W.-R. Wang, W.-L. Wang, and J.-W. Yeh: *J. Alloys Compd.*, 2014, vol. 589, pp. 143–52.
5. C.-J. Tong, M.-R. Chen, J.-W. Yeh, S.-J. Lin, S.-K. Chen, T.-T. Shun, and S.-Y. Chang: *Metall. Mater. Trans. A*, 2005, vol. 36A, pp. 1263–71.
6. W.-R. Wang, W.-L. Wang, S.-C. Wang, Y.-C. Tsai, C.-H. Lai, and J.-W. Yeh: *Intermetallics*, 2012, vol. 26, pp. 44–51.
7. C.-J. Tong, Y.-L. Chen, J.-W. Yeh, S.-J. Lin, S.-K. Chen, T.-T. Shun, C.-H. Tsau, and S.-Y. Chang: *Metall. Mater. Trans. A*, 2005, vol. 36A, pp. 881–93.
8. C.-C. Tung, J.-W. Yeh, T. Shun, S.-K. Chen, Y.-S. Huang, and H.-C. Chen: *Mater. Lett.*, 2007, vol. 61, pp. 1–5.
9. Y.-F. Kao, T.-J. Chen, S.-K. Chen, and J.-W. Yeh: *J. Alloys Compd.*, 2009, vol. 488, pp. 57–64.
10. C.-M. Lin and H.-L. Tsai: *Intermetallics*, 2011, vol. 19, pp. 288–94.
11. S. Singh, N. Wanderka, B.S. Murty, U. Glatzel, and J. Banhart: *Acta Mater.*, 2011, vol. 59, pp. 182–90.
12. M. Nahmany, Z. Hooper, A. Stern, V. Geanta, and I. Voiculescu: *Metall. Microstruct., Anal.*, 2016, vol. 5, pp. 229–40.
13. T. Yue, H. Xie, X. Lin, H. Yang, and G. Meng: *Entropy*, 2013, vol. 15, pp. 2833–45.
14. T.M. Yue, H. Xie, X. Lin, H.O. Yang, and G.H. Meng: *J. Alloys Compd.*, 2014, vol. 587, pp. 588–93.
15. B.A. Welk, R.E.A. Williams, G.B. Viswanathan, M.A. Gibson, P.K. Liaw, and H.L. Fraser: *Ultramicroscopy*, 2013, vol. 134, pp. 193–99.
16. A.C. Martin and C. Fink: *Weld. World*, 2019, vol. 63, pp. 739–50.
17. K. Poorhaydari, B.M. Patchett, and D.G. Ivey: *Weld. J.*, 2005, vol. 84, pp. 149s–55s.
18. B.T. Alexandrov and J.C. Lippold: *Weld. World*, 2013, vol. 57, pp. 635–48.
19. G. Vander Voort and E. Manilova: *Microsc. Microanal.*, 2004, vol. 10, pp. 690–1.
20. J.M. Sosa, D.E. Huber, B. Welk, and H.L. Fraser: *Integr. Mater.*, 2014, vol. 3, pp. 123–40.

Publisher's Note Springer Nature remains neutral with regard to jurisdictional claims in published maps and institutional affiliations.